Preprints (www.preprints.org) | NOT PEER-REVIEWED | Posted: 3 August 2022 doi:10.20944/preprints202208.0087.v1

Article

Piezoelectric Response and Substrate Effect of ZnO Nanowires for Mechanical Energy Harvesting in Internet of Things Applications

Mateusz Wlazło [1,*,†,‡], Maciej Haras [2,3,†], Grzegorz Kołodziej [1], Oliwia Szawcow [1], Jakub Ostapko [1], Wojciech Andrysiewicz [1], and Thomas Skotnicki [2,3,4]

1 CBRTP - Research and Development Center of Technology for Industry, Waryńskiego 3A, 00-645 Warsaw, Poland
2 Warsaw University of Technology, Centre for Advanced Materials and Technologies CEZAMAT, ul. Poleczki 19, 02-822 Warsaw, Poland
3 CENTERA Laboratories, Institute of High-Pressure Physics, Polish Academy of Sciences, Warsaw, 01-142, Poland
4 Warsaw University of Technology, Faculty of Electronics and Information Technology, Institute of Microelectronics and Optoelectronics, ul. Koszykowa 75, 00-662 Warsaw, Poland
* Correspondence: mateusz.wlazlo@ensemble3.eu
† These authors contributed equally to this work.
‡ Current address: Ensemble3 Centre of Excellence, Wólczyńska 133, 01-919 Warsaw, Poland

Abstract: The present experiment concerns deposition of ZnO by ALD and subsequent growth of nanowires by chemical bath. We used a novel AISI 301 steel substrate with mechanical parameters that make it suitable to use as a piezoelectric component in an energy harvesting device. We found out that a thin layer of another oxide below ZnO provides outstanding adhesion. Without it, ZnO exhibits island growth and is mechanically unstable. Such prepared samples were placed under repeated mechanical stress. They showed a piezoelectric signal which is stable after hundreds of actuations. This shows good promise for use of our device based on ZnO, an earth-abundant and non-toxic material, as an alternative to widespread in piezo components but environmentally unfriendly PZT. The piezo layers generated enough power for operations performed by a IoT chip. The designed measurement setup allowed for the demonstration of an application of AISI 301 steel substrate coated with ZnO by atomic layer and chemical bath deposition techniques as a piezoelectric component capable of generating energies usable in Internet of Things applications.

Keywords: piezoelectricity; energy harvesting; zinc oxide; nanostructures

1. Introduction

Since more than five decades the semiconductor industry continually astonishes the market with rising fabrication capacity (delivering more than 100 bn units in 2022) [1] under unprecedented cost effectiveness [2], dumping average transistor price more than x1000. This results in an average Compound Annual Growth Rate (CAGR) of 8.6% over 43 years timespan [3], a growth rate that has never been seen before (see Fig. 1(a)).

Recently, a new driver for the entire semiconductor industry has appeared that is the emerging market of the Internet of Things (IoT) [4]. IoT nodes already outnumber human population x6.4 and are expected to reach 70 bn units in 2030 [5] (see Fig. 1(b)). IoT market represents already a branch sized ∼\$1.6 bn [6,7] and exhibits outstanding average CAGR of ∼39% over 2015-2021 [8]. Surprisingly, the IoT growth could have been even faster, but it has been impaired by the lack of alternatives for battery and wire supply. The principle of IoT is to establish communication between small electronic devices, called Things, e.g. temperature sensors, presence detectors, pressure sensors, etc., distributed upon large area. Communication between Things omits human intervention [9]. Current challenges for IoT

Preprints (www.preprints.org) | NOT PEER-REVIEWED | Posted: 3 August 2022 doi:10.20944/preprints202208.0087.v1

include the size, portability, location spots and quantity of devices, and providing power supply for each IoT device node. Conventional supply (batteries or wires) is burdened with important drawbacks. Batteries require periodic checks and replacements if needed. This requires direct access to each of the nodes, and without significant breakthroughs would soon give full-time jobs for entire humanity. Additionally, batteries have a negative impact on the environment in the form of tons of used batteries trash. Wire supply is expensive and difficult to modify, which significantly reduces the portability and mobility of Things. Therefore, energy autonomy would be a huge relief for IoT, paving the way under future growth and expansion to the market.

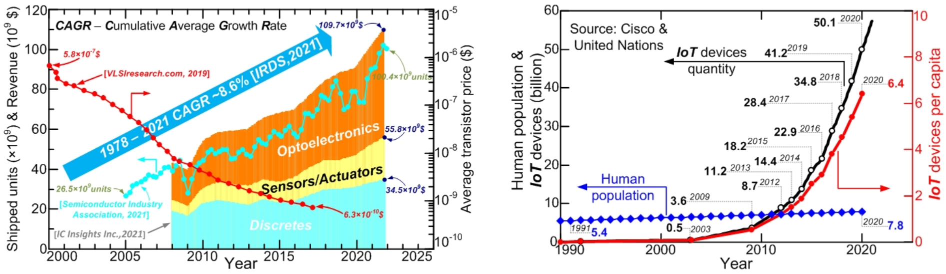

Figure 1. (**a**) History of the semiconductor industry underlining fabrication capability boost [1] (blue line), cost reduction [2] (red line), CAGR [3] (blue arrow), revenue per selected branch [10] (bar plot); (**b**) Historical comparison of IoT nodes quantity [5] (black line) with human population [11] (blue line), highlighting the IoT devices per capita (red line).

The fabrication capabilities boost, and cost reduction illustrated in Fig. 1(a) is accompanied by the galloping miniaturization (transistor's gate length reduced by factor x200) and performance boost (clock frequency increased x21000) (see Fig. 2(a)). Owing to this, modern electronic devices require less and less energy to operate. Over the last three decades, the energy consumption has decreased by a factor of almost 42000 for the same load.

These two industrial circumstances, IoT market growth and development of less energy-demanding devices, are driving the research towards alternative power supply enabling the elimination of wires and/or batteries. Development of micro- and nanotechnologies opened new possibilities to produce sufficient energy from wastes or naturally available energy sources. This approach defines the branch known as energy harvesting (EH) [12]. EH is nowadays gaining enormous attention from both industrials and academics, which is manifested by the number of filled patent applications and scientific publications (see Fig. 2(b)). A decrease in publications and patents after 2019 can be observed. It can be attributed to the pandemic of COVID-19 that confronted industrial and academic sectors with huge difficulties: cutting costs, production stoppages, temporary lab closure, remote work, confinements, etc. This effect is visible particularly in the share of conference papers which diminished greatly in 2020 and 2021. Nevertheless, the raising trend from before 2019 is expected to be reconstituted soon when the pandemic situation no longer affects industrial and academic working conditions.

 doi:10.20944/preprints202208.0087.v1

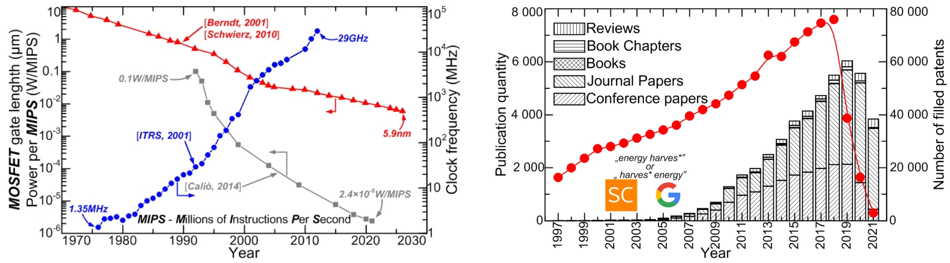

Figure 2. (**a**) Historical evolution of the electron devices performance revealing the miniaturization trend [13,14] (red line), operational frequency boost [15] (blue line) and reduction of power required per millions instruction per second (MIPS) [16] (gray line); (**b**) Development of the energy harvesting in number of scientific publications after Scopus (bar plot) and patent applications (red line) following Google Patents.

Fig. 3 summarizes decades of research and thousands of scientific publications highlighting main conventional EH techniques and illustrating the physics and input energy source.

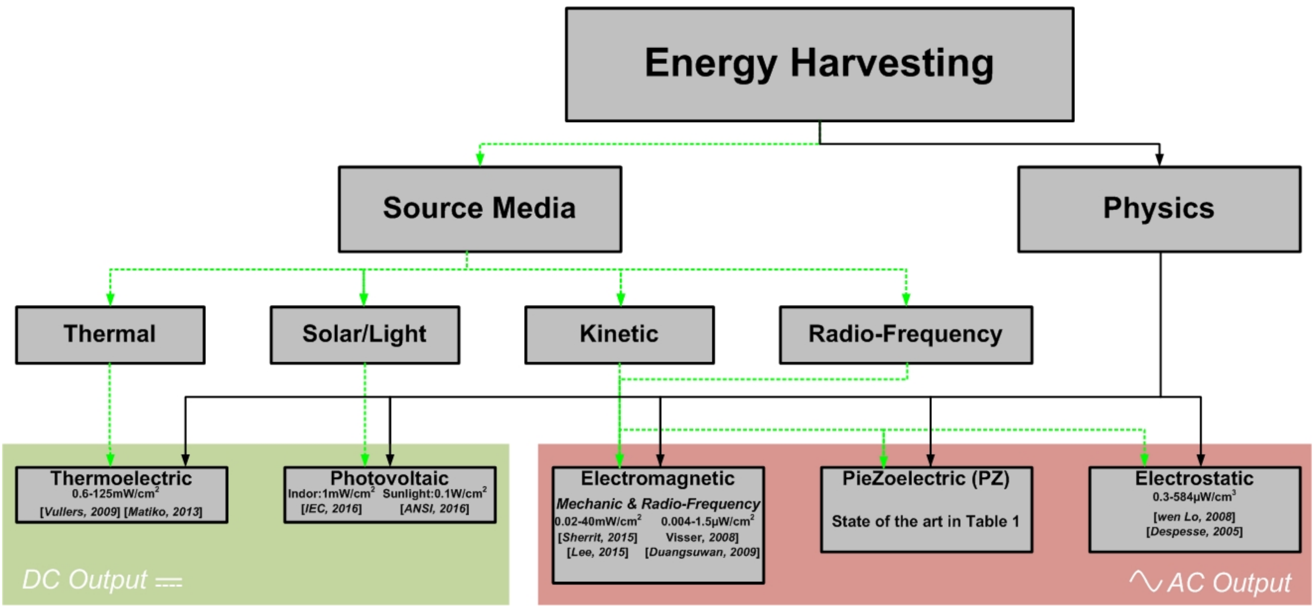

Figure 3. Taxonomy of the energy harvesting techniques with respect to the physical effect and input energy [17,18], highlighting common power densities for domestic environment reported in the literature; thermoelectric [19,20], photovoltaic [21,22], electromagnetic [23,24] (mechanical), [25,26] (radio-frequency), electrostatic [27,28]

Commenting on Fig. 3 it can be underlined that different energy sources require an adapted EH technique. Different physical effects and topologies are capable of producing different amounts of power. Confronting power densities in the range of μW or mW with power needed to supply modern electron devices (see Fig. 2(a) gray line) or modern IoT nodes requiring ∼10-100 μJ/cycle of operation [18,29,30], it can be concluded that well selected EH generator can totally cover the supply requirements of a modern IoT node offering energy-autonomous devices.

This paper focuses on one of the most common EH technique the PieZoelectric (PZ). A more focused literature review of PZ harvesters is provided in Table 1.

PZ converts mechanical energy (vibrations, stress) into electric voltage owing to the piezoelectric effect discovered in 1880 by Jacques and Pierre Curie [31]. This effect was observed in crystals such as tourmaline, topaz, calamine, and quartz but not in amorphous materials. The first application of this effect was the ultrasonic submarine detector constructed in France in 1917 [32].

Preprints (www.preprints.org) | NOT PEER-REVIEWED | Posted: 3 August 2022 doi:10.20944/preprints202208.0087.v1

Since their discovery, huge improvements in PZ materials have been obtained. This market of piezoelectric devices was estimated at $14.3 bn in 2010. The use of PZ materials is very wide, from well-known high voltage generators in lighters to infertility treatment [33]. Piezoelectrics are mainly used as sound sensors [34], as cantilevers in atomic force microscopes [35], noise and vibrations attenuators [36], motors [37], and, recently, as energy harvesters [19,38–40]. The piezoelectric effect is reversible. A mechanical deformation can be achieved by applying an electric potential to the material [40]. The reverse piezoelectric effect is very useful in various diagnostic applications e.g. wrist blood pressure or heart beat rate monitoring [41] it is also used to detect fatigue cracks in materials [42] e.g. wind turbines rotor blades [43].

PZ offers single-step conversion by directly transforming mechanical vibrations into electric potential. The material is therefore the crucial point of this conversion. The most popular piezoelectric material is the lead zirconium titanate (PZT) [44–57]. Its high cost and lead (Pb) content have motivated research on alternative materials. A widely studied example is zinc oxide which is composed of abundant and non-toxic elements. Of particular note is the possible synthesis in the form of unidirectional nanowires [58–62] which enhances the piezoelectric effect in the preferred axis. The directionallity of the nanowires highly depends on the substrate on which they are grown, which is also an important issue concerning current results described further in the text.

Table 1. Summary of reported piezoelectric harvesters and their parameters

f (Hz)	**Excitation** (m/s^2)	**Mass** (g)	**Volume** (cm^3)	**P** (μW)	**Power density** ($\mu W/cm^3$)	**Material**	**Reference**
0.5	N/A	1.2	0.101	0.25	2.47	PZT-5H	[52]
1.1	N/A	N/A	25	8400	336	PZT	[44]
100	72.7	0.96	0.20	35.5	16.3	PZT	[48]
120	2.5	9.2	1	375	375	PZT	[46]
120	0.98	N/A	N/A	500	N/A	PMNZT	[63]
13.9	106	N/A	$27 \cdot 10^{-6}$	1	$37.04 \cdot 10^3$	PZT	[49]
1500	3.92	$9 \cdot 10^{-4}$	0.005	0.03	60	AlN	[64]
230	9.8	N/A	N/A	0.27	N/A	PZT	[55]
40	2.5	52.2	4.8	1700	700	PZT	[50]
462.5	19.6	N/A	N/A	2.15	N/A	PZT	[56]
50	N/A	N/A	9	180	20	PZT	[51]
56	N/A	228	113	$1 \cdot 10^5$	2650	P1-89 PZT	[54]
608	9.8	0.0016	0.0006	2.16	3600	PZT	[53]
67	4	2.8	0.987	240	243.1	PZT	[57]
7000	N/A	N/A	N/A	1600	N/A	PZT-PIC255	[47]
80	2.3	0.8	0.128	2.1	16.4	PZT	[45]
N/A	N/A	N/A	0.045	1.03	22.8	ZnO NWs	[62]
N/A	N/A	N/A	$0.13 \cdot 10^{-3}$	$0.1 \cdot 10^{-3}$	1.28	ZnO NWs on paper	[60]
N/A	N/A	N/A	N/A	N/A	$1 \cdot 10^{-3}$	ZnO NWs	[58]
N/A	N/A	N/A	N/A	N/A	10	ZnO NWs	[59]
3	N/A	N/A	N/A	N/A	144	ZnO NWs	[61]
1.63	N/A	N/A	$4.51 \cdot 10^{-4}$	$1.38 \cdot 10^{-3}$	3.1	ZnO NWs on steel	(this work)

PZT – Lead zirconium titanate, $Pb[Zr_xTi_{1-x}]O_3$,
PMNZT – PZT co-doped with Mg and Nb,
ZnO NWs – zinc oxide nanowires,
N/A – data not available

Preprints (www.preprints.org) | NOT PEER-REVIEWED | Posted: 3 August 2022 doi:10.20944/preprints202208.0087.v1

2. Materials and Methods

2.1. Sample fabrication

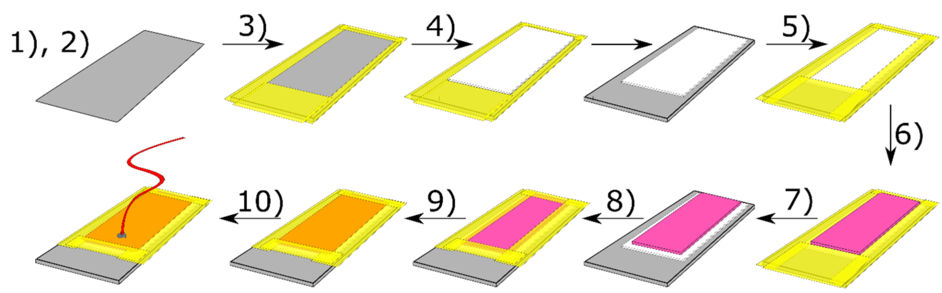

Figure 4. Manufacturing of the sample. **(1)** Cutting substrate (steel) into desired dimensions, **(2)** Degreasing and chemical cleaning of the substrate, **(3)** Masking of the substrate with Kapton tape prior to ALD deposition, **(4)** Deposition of adhesion layer and seeding layer via ALD on metal substrate. Materials employed were Al_2O_3 and ZnO, **(5)** Masking of the substrate with Kapton tape prior to hydrothermal growth, **(6)** Hydrothermal growth of ZnO NWs via hydrothermal method on exposed seeded surface, **(7)** Cleaning from unwanted residues, **(8)** Masking of the sample with Kapton tape before mounting of top electrode, **(9)** Placing and immobilization of top copper electrode to achieve contact only with Kapton tape and surface of ZnO nanowires, **(10)** Wiring of the top electrode.

2.1.1. Substrate

For piezoelectric material deposition, austenitic-ferritic stainless steel (EN 1.4310 / AISI 301 class) was chosen as the substrate due to its particular mechanical properties. This type of steel exhibits high yield strength and retention of shape after prolonged application of strain. The raw material in the form of 100 μm-thick sheets was cut into rectangular 20 x 50 mm samples. The substrate itself acted as the bottom electrode. It should be noted that a device with optimized substrate resistivity may have offered better PZ efficiency at the cost of inferior mechanical properties.

The AISI 301 steel is a novel type of substrate. For verification of growth conditions, selected processes were performed additionally on polished silicon (Si) substrates. If not otherwise explicitly indicated, we will refer to samples deposited on the steel substrate.

2.1.2. Synthesis

The following textual description of synthesis steps is illustrated in Fig. 4 in graphical form. After cutting to desired dimensions, the steel substrates were masked using Kapton tape resulting in a 18 x 35 mm exposed surface. Then, ALD layers were deposited. The role of ALD deposition was to enable the growth of piezoelectric ZnO nanowires (NWs) while ensuring good adhesion to the bottom electrode surface. ALD deposition was performed using Beneq P-400 reactor kept heated to 200 °C throughout the processes. Diethylzinc (DEZ) [Lanxess, CAS 557-20-0, purity $\geq$ 99.5 % m/m], trimethylaluminum (TMA) [Lanxess, CAS 75-24-1, purity $\geq$ 99.8 % m/m] and deionized water (H_2O) were used as zinc, aluminum and oxygen precursors. The reagents were kept at room temperature with the exception of H_2O which was heated to a constant temperature of 28 °C. Nitrogen gas (99.99% N_2) with a flow rate of 2500 sccm (square cubic centimeter per minute) was used as a carrier and purge gas. Aluminum oxide (Al_2O_3) films were obtained by sequential dosing of H_2O for 350 ms and TMA for 300 ms. The pulses were separated by a 3 s purges of N_2. This cycle was repeated a set number of times to obtain a desired thickness (assuming thickness growth per cycle GPC_{Al2O3} = 0.1 nm). Zinc oxide (ZnO) films were deposited in a similar manner by dosing H_2O for 350 ms and DEZ for 300 ms with a 3 s purge of N_2 between precursor pulses (GPC_{ZnO} = 0.167 nm). At the end of each process, a 600 ms pulse of H_2O was delivered to ensure full oxygen saturation, followed by a 10 s N_2 purge.

Preprints (www.preprints.org) | NOT PEER-REVIEWED | Posted: 3 August 2022 doi:10.20944/preprints202208.0087.v1

Chemical bath deposition (CBD) was performed by placing the samples on which ALD layers were deposited in an aqueous solution of zinc nitrate hexahydrate $Zn(NO_3)_2 \cdot 6H_2O$ [Chempur] and hexamethylenetetramine (HMT, $C_6H_{12}N_4$) [Thermo Scientific]. The solution concentration varied between 30 and 100 mM. The molar ratio of the reagents was kept constant at 1:1, replicating the conditions described in Refs. 65,66. For each of the processes, the samples were left in the solution for 4 hours. The reaction containers were placed on a heated surface – a hotplate or a magnetic stirrer, in both cases set to 95 °C. After the deposition process the samples were rinsed with DI water for 5 minutes in an ultrasonic bath.

Finally, the samples were once again masked with Kapton tape resulting in a 16 x 32 mm exposed surface that was put into contact with a copper electrode which acted as the top electrode.

2.2. Characterization

2.2.1. SEM

Scanning electron microscopy (SEM) was performed using the Thermo Fisher Phenom Pharos system. The system is equipped with energy-dispersive X-ray spectroscopy (EDS) attachment which was used to confirm the presence of expected layers by analyzing Zn and O content on the surface. The applied electron beam acceleration voltage was 12–15 kV (imaging mode) or 5 kV (EDS mode).

The morphology of NWs produced by using the hotplate was found to be more uniform than when using the stirrer. There was a difference in the amount of scattered aggregates whose dimensions were much larger than the NWs themselves (see Fig. 5). The resulting inhomogeneity is generally believed detrimental to piezoelectrical properties of the sample. Conversely, a continuous coating of uniformly-shaped and highly-oriented structures is seen as desirable [67]. Such a uniform and oriented coating was obtained on silicon substrates used to verify growth conditions (see Fig. 6).

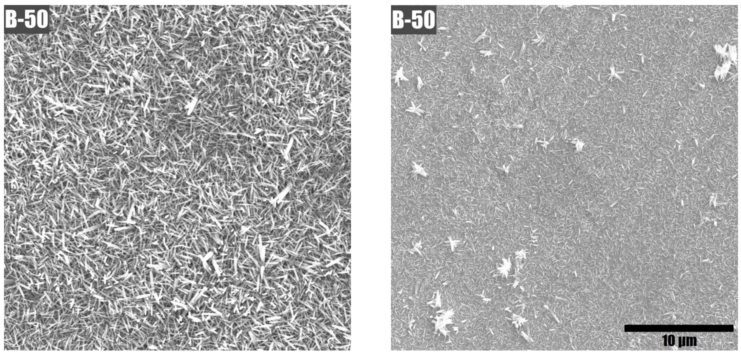

Figure 5. Scanning electron top-view micrographs of sample B-50 showing the ZnO nanowires on samples coming from a process carried out in a container vessel placed on a hotplate (left) and on a heated magnetic stirrer (right).

 doi:10.20944/preprints202208.0087.v1

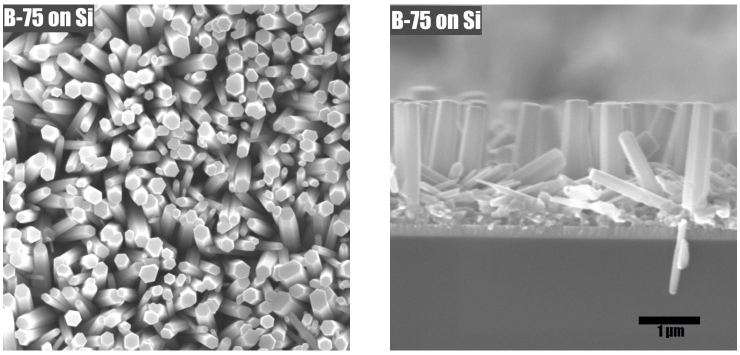

Figure 6. Scanning electron top-view and cross-section micrographs of sample B-75 deposited on silicon.

2.2.2. Piezoelectric effect measurements

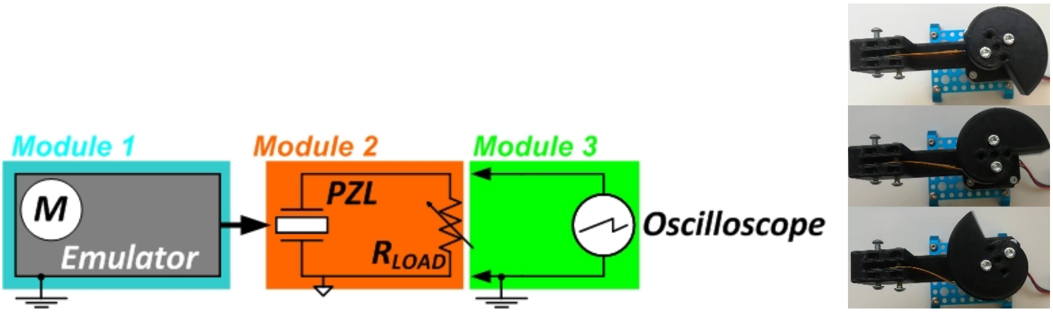

Figure 7. Electrical diagram of the test bench utilized for the evaluation of piezoelectric response of ZnO samples under repeated mechanical deformation (left) and snapshots showing the action performed by the spiral actuator.

The first module (leftmost in Fig. 7), called the emulator, consisted of an actuator which applied mechanical strain to the sample. The actuator was designed in the shape that can be approximated by the logarithmic spiral equation r = $aexpk\phi$ (with a > 0), starting at ϕ=0 and ending at ϕ=2nπ (n=1,2,...). The spiral actuator manufactured by 3D printing (ABS filament) was mounted horizontally on the shaft of a step motor (Makeblock 42BYG) through a hole in the middle, in such a manner that the rotation of the shaft resulted in rotation of the actuator. The step motor was controlled by a single-board computer (Raspberry Pi) running Raspbian OS.

The role of the second module was to provide a mounting point for the sample (middle of Fig. 7). Rectangular samples were placed inside a clamp by on of its shorter sides. The clamp has electrical contact only with the bottom electrode (steel substrate). To facilitate electrical contact to the sample, bottom electrode was additionally tightly screwed to the clamp. An electrode made from a sheet of copper cut to the dimensions of the sample and attached on top was wired directly to the measurement system. The clamp itself was placed on a rectangular ABS part that acted as an insulating table that eliminated possible contact between the metal clamp and frame.

The two modules were attached to a shared construction frame. The distance between the actuator and the sample could be adjusted without disconnecting the sample. This allowed performing measurements on samples with different dimensions. In addition, changing the distance can aid in adjusting the intensity of mechanical actuation delivered to the sample.

The rotation of the spiral shape allowed to deliver two kinds of strain to the sample. In the first mode, the sample is bent and unbent at an angle and speed controlled in a precise manner by step motor programming and the adjustable distance to the sample. In the second mode, the spiral is rotated beyond the endpoint which results in the sample being gradually bent and then rapidly released.

The third module was the measurement and data acquisition system (rightmost in Fig. 7). Its main hub was a Keysight DSOX2024A oscilloscope connected in parallel to the second module through a variable resistive load realized by a resistance box. During one measurement cycle, the load was first set to the maximum available load R_{MAX}=1.111111·$10^7\Omega$ and then gradually reduced by turning one knob of the resistance box at a time down to R_{MIN}=2.111·$10^4\Omega$. The values of R_{MAX} and R_{MIN} were chosen based on the expected impedance of the sample between R_{LOAD}=10^6-10^7 Ω.

The data was saved in the form of voltage waveform vs. time V(t) for further analysis. A fragment of one of the typical waveforms generated by our samples when displaced by the emulator module is displayed in Fig. 8. It was recorded at optimal external load, i.e. the one under which the calculated generated energy was the highest.

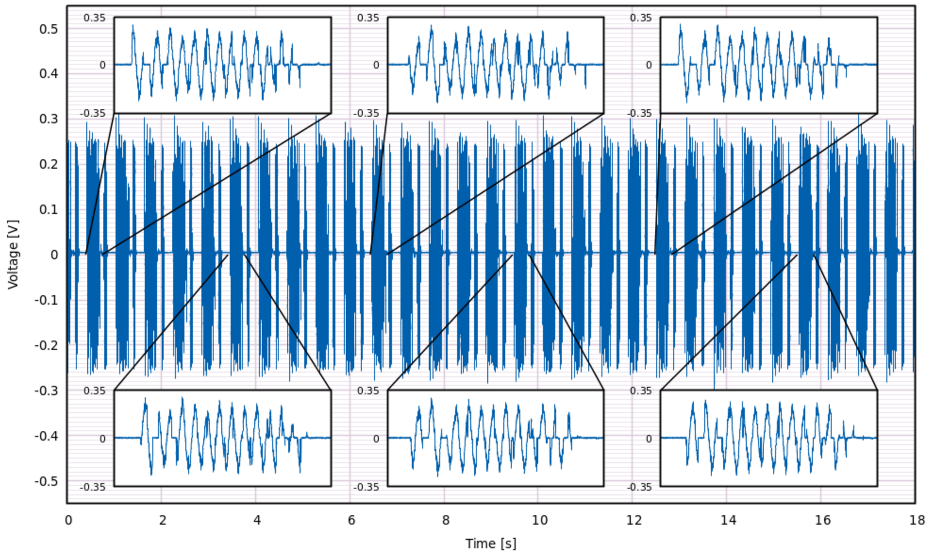

Figure 8. Voltage waveform generated by sample B-75 under R_{LOAD}=6.11 MΩ upon repeated actuation under test conditions. Insets show waveforms of single subsequent actuations. The length of a single displayed waveform is 0.5 s and the start points between subsequent actuations are separated by 0.61 s.

3. Results and discussion

Table 2. This is a table caption. Tables should be placed in the main text near to the first time they are cited.

Sample ID	**ALD seed layer**	**Reaction solution concentration** (mM/dm^3)
A-100	200 nm ZnO (**A**)	100
A-30	200 nm ZnO (**A**)	30
B-75	20 nm Al_2O_3 / 200 nm ZnO (**B**)	75
B-50	20 nm Al_2O_3 / 200 nm ZnO (**B**)	50

Preprints (www.preprints.org) | NOT PEER-REVIEWED | Posted: 3 August 2022 doi:10.20944/preprints202208.0087.v1

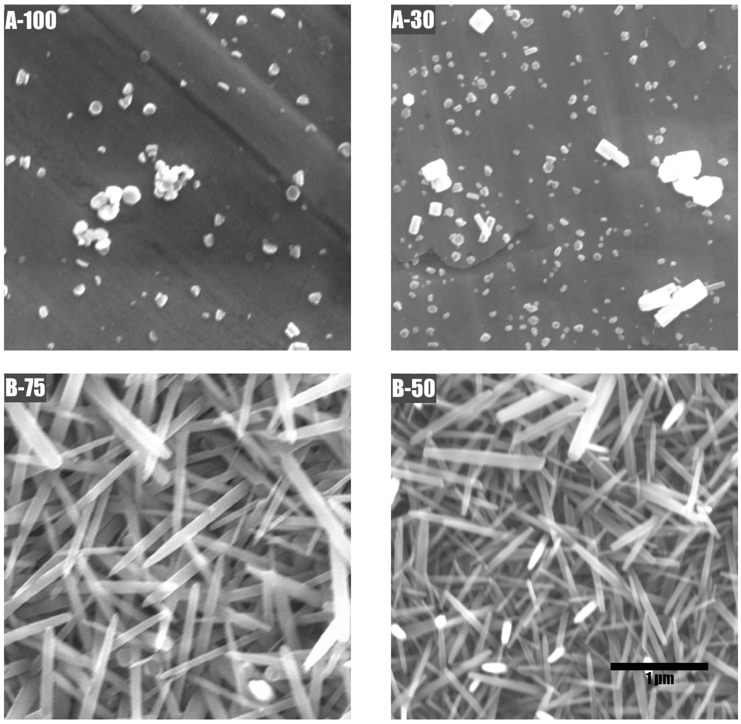

Figure 9. Scanning electron top-view micrographs of sample A-100 (top left), A-30 (top right), B-75 (bottom left), B-50 (bottom right).

The ALD and CBD processes have been performed on samples including the full size AISI 301 steel substrates, as well as on smaller pieces which were used for SEM imaging. The processes were carried out with heating provided by a hotplate. Two types of ALD layers were used as seed layers. The first type, labelled **A** constituted of ∼200 nm ZnO layers.Fig. 9 shows magnified images of each of the four samples (A-100, A-30, B-75, B-50) which display the different growth mode depending on the type of ALD layer. It reveals that the growth of nanowires on such type **A** seed layer was minimal and scattered in very few randomly distributed sites on the surface. On the other hand, ALD layer labelled **B** provided adequate conditions for uniform growth of nanowires.

SEM images were used to calculate the volume of the active layer, which was the nused to estimate the generated power density in piezoelectric effect generation measurements. ZnO grown in the form of nanowires features considerable space gaps between each individual nanowire. Using the cross-section image, the typical length of a single nanowire was estimated to be $\sim$2 μm, amounting together with the seed layer of 200 nm to the total possible thickness of $\sim$2.2 μm

As evidenced by SEM images (eg. on Figure 5(a)), in contrast to the crystalline silicon substrate, ZnO nanowires on AISI 301 substrate grow in a more disoriented manner. The nanowires appear to grow at an angle to the surface. This is attributed to the lack of uniform crystal structure of the substrate. Similarly to the Si substrate, there is a considerable amount of gap space between the wires. Taken these aspects into account, the filling factor of the active layer was estimated at 40% for power density calculations. Thus the volume of the piezo-active layer used for power density calculations was equal to $16mm \times 32mm \times 2\mu m \times 0.4 = 4.51 \cdot 10^{-4}$ cm^3.

Preprints (www.preprints.org) | NOT PEER-REVIEWED | Posted: 3 August 2022 doi:10.20944/preprints202208.0087.v1

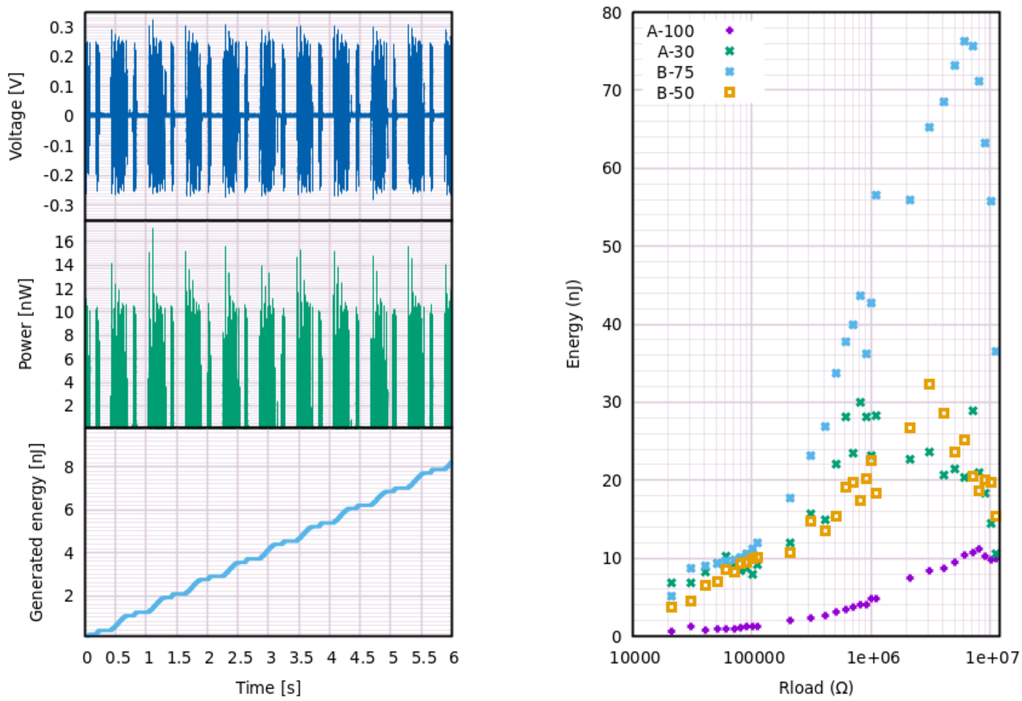

Figure 10. (**a**) Recorded waveform V(t) (top), instantaneous power $P(t) = V^2(t)/R_{LOAD}$ (middle) and accumulated energy calculated by numerically integrating the signal $E(T) = \int_0^T P(t)dt = \int_0^T V^2(t)dt/R_{LOAD}$ (bottom) for sample B-75; (**b**) Energy accumulated in a single production run of 90 actuations vs. resistive load.

Using the voltage recorded for each sample, instantaneous power was computed according to Ohm's law, $P(t) = V^2(t)/R_{LOAD}$, where R_{LOAD} is the resistive load set on the resistance box. Then the value of energy accumulated from the beginning of the measurement up to t=T was computed by numerical integration of power with respect to time, $E(T) = \int_0^T P(t)dt = \int_0^T V^2(t)dt/R_{LOAD}$ (see Figure 10(a)).

Recorded waveforms included the signal generated by piezoelectric samples as well as a certain amount of noise. Both of these types of waveforms were integrated when computing the generated energy. For higher values of R_{LOAD}, the contribution of noise was negligible. However, when lower values of R_{LOAD} were used, even the low voltage values contributed significantly to the integrated energy. This was alleviated by introducing a cutoff value V_{CUTOFF}. Below this value the recorded voltages were ignored as if V(T) was equal to 0. Cutoff values between 0 to 5 mV were tested. It has been found that V_{CUTOFF} = 5 mV was the appropriate setting, taking into account that the undesired influence of noise at low R_{LOAD} values was mitigated while keeping energies computed at high R_{LOAD} essentially unchanged. The high signal-to-noise ratio shows that the samples and experimental setup were well-prepared.

Waveforms were recorded at each R_{LOAD} value for a total of 55.2 seconds. During this period, the samples were displaced 90 times by the emulator, resulting in actuation frequency equal to 1.63 Hz. This procedure was repeated at 30 different values of R_{LOAD}, amounting to a total of 2700 mechanical actuations delivered to each sample. Across the measurements the voltage signal was stable.

The amount of accumulated energy is displayed in Figure 10(b) as a function of resistive load connected to each sample. For each of the measured samples, a maximum value of accumulated energy was obtained at a certain resistive load R_{LOAD} value. This is the value in which the internal impedance of the sample is matched to the external impedance of R_{LOAD}. Depending on the sample, the matched impedance value was

 doi:10.20944/preprints202208.0087.v1

between 0.81 and 8.11 MΩ. It should be noted, however, that the Energy-load profile is the most spread-out for the sample that appears to have the lowest impedance, A-30. The power was just 0.02 nW lower at R_{LOAD} = 7.11 MΩ. This would place it much closer to impedance-matched conditions measured for other samples. Other samples, in particular type-**B** have a more clearly defined maxima. This leads us to believe that for these two samples the highest energy points indeed correspond to impedance-matched conditions.

The highest amount of energy is generated by sample B-75 – 76.37 nJ at the optimal setting of the resistive box. This corresponds to the amount of power equal to 1.38 nW. Taking into account the volume of active layer, the power density can be calculated at 3.1 μW/cm^3. Compared to other reported piezoelectric harvesters (see Table 1), this value places it in the middle of reported power densities for harvesters based on ZnO nanowires. It is slightly higher but comparable to ZnO synthesized on a paper substrate, which is also a flexible substrate similarly to deposition on AISI 301 steel reported here, and may serve similar applications in mechanical energy harvesting.

Devices which draw few nW sleep power and 16 pJ per transmitted bit are realized in research wireless sensors [52]. These could be powered easily by a small array of piezoelectric devices described here. The growth methods also allow for the deposition of a thicker layer (ALD) or vertically stacked structures [68]. Both of these options might be engineered to contribute an increased piezo-voltage in future applications.

Table 3. Piezoelectric energy generation parameters obtained from measurements of voltage generated by the samples.

Sample ID	**Optimal impedance** MΩ	**Max. accumulated energy** nJ	**Max. power** nW	**Max. accumulated energy density** μJ/cm^3	**Max. power density** μW/cm^3
A-100	0.81	29.94	0.54	66.5	1.2
A-30	8.11	11.18	0.20	24.8	0.4
B-75	6.11	76.37	1.38	169.5	3.1
B-50	3.11	32.36	0.58	71.8	1.3

4. Conclusions

In this work, we have demonstrated growth of ZnO nanowires from chemical bath on a novel type of substrate – AISI 301 steel. The substrate was chosen with mechanical energy harvesting applications in mind. After its deposition, the measured voltage upon repeated mechanical actuation provided the means of verifying its applicability in Internet of Things applications.

The nanostructured active layer was deposited directly on the substrate which was first prepared by seeding process using atomic layer deposition of thin oxides. A typical procedure in which pure zinc oxde is used as seed layer to catalyze the nanowire growth has been modified to account for the particular surface properties of the AISI 301 substrate. The seed layer modification by inserting a 20 nm-thick layer of another oxide Al_2O_3 was found to eliminate adhesion issues of the ZnO ALD layer.

The measured voltage signal was stable upon thousands of actuations of each sample, confirming the resilience of the piezo layer to sustained mechanical stress. Moreover, the piezo-active layer generated a considerable amount of power, enough for typical operations performed by IoT devices. The power density was comparable to other reported values (see Table 1). In particular it was on the same order of magnitude as ZnO nanowires fabricated on another type of flexible substrate [60]. These two factors, when combined, show high promise for final application of the device as apart of a power generation component for a IoT wireless sensor node.

Author Contributions: conceptualization, T.S. and M.H.; formal analysis, M.W., M.H. and G.K.; investigation, G.K., O.S., M.W., J.O. and M.H.; methodology, M.H., M.W. and W.A.; software, W.A.; supervision, T.S.; visualization, M.W. and G.K.; writing—original draft preparation, M.W. and M.H.; writing—review and editing, M.W., M.H. and T.S. All authors have read and agreed to the published version of the manuscript.

Funding: This research was funded by the project PULSE-COM of the European Union's Horizon 2020 research and innovation programme under grant agreement No 863227.

Conflicts of Interest: The authors declare no conflict of interest.

1. 2021 state of the U.S. semiconductor industry. Technical report, Semiconductor Industry Association, 2021.
2. Is it time for a revolution? https://www.vlsiresearch.com/. Accessed: 2022-01-17.
3. IRDS 2021: Executive Summary. Technical report, IEEE-International Roadmap for Devices and Systems (IRDS), 2021.
4. Al-Fuqaha, A.; Guizani, M.; Mohammadi, M.; Aledhari, M.; Ayyash, M. Internet of Things: A Survey on Enabling Technologies, Protocols, and Applications. *IEEE Communications Surveys & Tutorials* **2015**, *17*, 2347–2376. https://doi.org/10.1109/comst.2015.2444095.
5. Farber, D. Counting the Internet of things in real time. https://www.cnet.com/science/counting-the-internet-of-things-in-real-time/. Accessed: 2022-06-23.
6. Columbus, L. Roundup Of Internet Of Things Forecasts And Market Estimates, 2016. https://www.forbes.com/sites/louiscolumbus/2016/11/27/roundup-of-internet-of-things-forecasts-and-market-estimates-2016/. Accessed: 2022-06-23.
7. Press, G. Internet of Things by the numbers: Market estimates and forecasts. http://www.forbes.com/site of-things-by-the-numbers-market-estimates-and-forecasts. Accessed: 2022-06-23.
8. IRDS 2021: Executive Summary. Technical report, IoT Analytics, 2018.
9. An Introduction to Internet of Things (IoT) and Lifecycle Management – Interoperability Architecture and Standards. http://www.opengroup.org/iot/iotwp/p3.htm. Accessed: 2022-06-20.
10. The 2022 McClean Report, A complete Analysis and forecast of the semiconductor industry. Technical report, IC Insights Inc., 2021.
11. World Population Prospects 2019. Technical report, Department of Economic and Social Affairs, Population Division, 2019.
12. Briand, D.; Yeatman, E.; Roundy, S.; Brand, O.; Fedder, G.; Hierold, C.; Korvink, J.; Tabata, O. *Micro Energy Harvesting*; Advanced Micro and Nanosystems, Wiley, 2015.
13. Berndt, E.R.; Rappaport, N.J. Price and Quality of Desktop and Mobile Personal Computers: A Quarter-Century Historical Overview. *American Economic Review* **2001**, *91*, 268–273. https://doi.org/10.1257/aer.91.2.268.
14. Schwierz, F. Graphene transistors. *Nature Nanotechnology* **2010**, *5*, 487–496. https://doi.org/10.1038/nnano.2010.89.
15. International Technology Roadmap for Semiconductors 2001 (updated 2002). Technical report, International Roadmap Commitee, 2002.
16. Richards, M.; Shaw, G. Chips, Architectures and Algorithms: Reflections on the Exponential Growth of Digital Signal Processing Capability **2004**.
17. Caliò, R.; Rongala, U.; Camboni, D.; Milazzo, M.; Stefanini, C.; de Petris, G.; Oddo, C. Piezoelectric Energy Harvesting Solutions. *Sensors* **2014**, *14*, 4755–4790. https://doi.org/10.3390/s140304755.
18. Haras, M.; Skotnicki, T. Thermoelectricity for IoT – A review. *Nano Energy* **2018**, *54*, 461–476. https://doi.org/10.1016/j.nanoen.2018.10.013.
19. Vullers, R.; van Schaijk, R.; Doms, I.; Hoof, C.V.; Mertens, R. Micropower energy harvesting. *Solid-State Electronics* **2009**, *53*, 684–693. https://doi.org/10.1016/j.sse.2008.12.011.
20. Matiko, J.W.; Grabham, N.J.; Beeby, S.P.; Tudor, M.J. Review of the application of energy harvesting in buildings. *Measurement Science and Technology* **2013**, *25*, 012002. https://doi.org/10.1088/0957-0233/25/1/012002.
21. IEC 61215-1-1: Terrestrial photovoltaic (PV) modules - Design qualification and type approval - Part 1: Test requirements. International standard, International Electrotechnical Commission (IEC), 2016.
22. 90.1-2016: Energy Standard for Buildings Except Low-Rise Residential Buildings. International standard, ANSI/ASHRAE/IES, 2016.

23. Sherrit, S.; Lee, H.J.; Walkemeyer, P.; Winn, T.; Tosi, L.P.; Colonius, T. Fluid flow nozzle energy harvesters. In Proceedings of the SPIE Proceedings; Lynch, J.P., Ed. SPIE, 2015. https://doi.org/10.1117/12.2084574.
24. Lee, H.; Sherrit, S.; Tosi, L.; Walkemeyer, P.; Colonius, T. Piezoelectric Energy Harvesting in Internal Fluid Flow. *Sensors* **2015**, *15*, 26039–26062. https://doi.org/10.3390/s151026039.
25. Visser, H.J.; Reniers, A.C.F.; Theeuwes, J.A.C. Ambient RF Energy Scavenging: GSM and WLAN Power Density Measurements. In Proceedings of the 2008 38th European Microwave Conference. IEEE, 2008. https://doi.org/10.1109/eumc.2008.4751554.
26. Duangsuwan, S.; Leukachorn, T.; Chinsawatpan, S.; Promwong, S. Experimental study for polarimetric measurement of RFID transfer function with in an indoor environment. In Proceedings of the 2009 IEEE 9th Malaysia International Conference on Communications (MICC). IEEE, 2009. https://doi.org/10.1109/micc.2009.5431410.
27. Lo, H.W.; Tai, Y.C. Parylene-based electret power generators. *Journal of Micromechanics and Microengineering* **2008**, *18*, 104006. https://doi.org/10.1088/0960-1317/18/10/104006.
28. Despesse, G.; Jager, T.; Jean-Jacques, C.; Léger, J.M.; Vassilev, A.; BASROUR, S.; Charlot, B. Fabrication and characterization of high damping electrostatic micro devices for vibration energy scavenging. *Proc. Design, Test, Integration and Packaging of MEMS and MOEMS* **2005**, pp. 386–390.
29. Markiewicz, M.; Wielgosz, M.; Bochenski, M.; Tabaczynski, W.; Konieczny, T.; Kowalczyk, L. Predictive Maintenance of Induction Motors Using Ultra-Low Power Wireless Sensors and Compressed Recurrent Neural Networks. *IEEE Access* **2019**, *7*, 178891–178902. https://doi.org/10.1109/access.2019.2953019.
30. Markiewicz, M.; Dziurdzia, P.; Konieczny, T.; Skomorowski, M.; Kowalczyk, L.; Skotnicki, T.; Urard, P. Software Controlled Low Cost Thermoelectric Energy Harvester for Ultra-Low Power Wireless Sensor Nodes. *IEEE Access* **2020**, *8*, 38920–38930. https://doi.org/10.1109/access.2020.2975424.
31. Schils, R. Pierre Curie. In *How James Watt Invented the Copier: Forgotten Inventions of Our Great Scientists*; SpringerLink : Bücher, Springer New York, 2011.
32. Katzir, S. Who knew piezoelectricity? Rutherford and Langevin on submarine detection and the invention of sonar. *Notes and Records of the Royal Society* **2012**, *66*, 141–157. https://doi.org/10.1098/rsnr.2011.0049.
33. Baltaci, V.; Özge Üner Ayvaz.; Ünsal, E.; Aktaş, Y.; Baltacı, A.; Turhan, F.; Özcan, S.; Sönmezer, M. The effectiveness of intracytoplasmic sperm injection combined with piezoelectric stimulation in infertile couples with total fertilization failure. *Fertility and Sterility* **2010**, *94*, 900–904. https://doi.org/10.1016/j.fertnstert.2009.03.107.
34. Manbachi, A.; Cobbold, R.S.C. Development and Application of Piezoelectric Materials for Ultrasound Generation and Detection. *Ultrasound* **2011**, *19*, 187–196. https://doi.org/10.1258/ult.2011.011027.
35. Gautsch, S.; Staufer, U.; Akiyama, T.; Hidber, H.R.; Tonin, A.; Howald, L.; Müller, D.; Niedermann, P.; de Rooij, N.F. Miniaturized atomic force microscope for planetary exploration. In Proceedings of the 9th European Space Mechanisms and Tribology Symposium; Harris, R.A., Ed., 2001, Vol. 480, *ESA Special Publication*, pp. 11–16.
36. Nandi, A.; Neogy, S.; Bhaduri, S.; Irretier, H. Vibration Attenuation by a Combination of a Piezoelectric Stack and a Permanent Magnet. *Shock and Vibration* **2012**, *19*, 719–734. https://doi.org/10.1155/2012/358953.
37. Inaba, R.; Tokushima, A.; Kawasaki, O.; Ise, Y.; Yoneno, H. Piezoelectric Ultrasonic Motor. In Proceedings of the IEEE 1987 Ultrasonics Symposium. IEEE, 1987. https://doi.org/10.1109/ultsym.1987.199059.
38. *Piezoelectric Energy Harvesting*; John Wiley & Sons, Ltd, 2011. https://doi.org/10.1002/9781119991151.fmatter.
39. Harb, A. Energy harvesting: State-of-the-art. *Renewable Energy* **2011**, *36*, 2641–2654. https://doi.org/10.1016/j.renene.2010.06.014.
40. Briscoe, J.; Dunn, S. *Nanostructured Piezoelectric Energy Harvesters*; SpringerBriefs in Materials, Springer International Publishing, 2014.
41. Li, Z.; Wang, Z.L. Air/Liquid-Pressure and Heartbeat-Driven Flexible Fiber Nanogenerators as a Micro/Nano-Power Source or Diagnostic Sensor. *Advanced Materials* **2010**, *23*, 84–89. https://doi.org/10.1002/adma.201003161.

42. Sohn, H.; Kim, S.B. Development of dual PZT transducers for reference-free crack detection in thin plate structures. *IEEE Transactions on Ultrasonics, Ferroelectrics and Frequency Control* **2010**, *57*, 229–240. https://doi.org/10.1109/tuffc.2010.1401.
43. Taylor, S.G.; Farinholt, K.; Choi, M.; Jeong, H.; Jang, J.; Park, G.; Lee, J.R.; Todd, M.D. Incipient crack detection in a composite wind turbine rotor blade. *Journal of Intelligent Material Systems and Structures* **2013**, *25*, 613–620. https://doi.org/10.1177/1045389x13510788.
44. Shenck, N.; Paradiso, J. Energy scavenging with shoe-mounted piezoelectrics. *IEEE Micro* **2001**, *21*, 30–42. https://doi.org/10.1109/40.928763.
45. White, N.M.; Glynne-Jones, P.; Beeby, S.P. A novel thick-film piezoelectric micro-generator. *Smart Materials and Structures* **2001**, *10*, 850–852. https://doi.org/10.1088/0964-1726/10/4/403.
46. Roundy, S.; Wright, P.K.; Rabaey, J. A study of low level vibrations as a power source for wireless sensor nodes. *Computer Communications* **2003**, *26*, 1131–1144. https://doi.org/10.1016/s0140-3664(02)00248-7.
47. Lu, F.; Lee, H.P.; Lim, S.P. Modeling and analysis of micro piezoelectric power generators for micro-electromechanical-systems applications. *Smart Materials and Structures* **2003**, *13*, 57–63. https://doi.org/10.1088/0964-1726/13/1/007.
48. Ng, T.H.; Liao, W.H. Sensitivity Analysis and Energy Harvesting for a Self-Powered Piezoelectric Sensor. *Journal of Intelligent Material Systems and Structures* **2005**, *16*, 785–797. https://doi.org/10.1177/1045389x05053151.
49. Jeon, Y.; Sood, R.; h. Jeong, J.; Kim, S.G. MEMS power generator with transverse mode thin film PZT. *Sensors and Actuators A: Physical* **2005**, *122*, 16–22. https://doi.org/10.1016/j.sna.2004.12.032.
50. Roundy, S.; Leland, E.; Baker, J.; Carleton, E.; Reilly, E.; Lai, E.; Otis, B.; Rabaey, J.; Sundararajan, V.; Wright, P. Improving Power Output for Vibration-Based Energy Scavengers. *IEEE Pervasive Computing* **2005**, *4*, 28–36. https://doi.org/10.1109/mprv.2005.14.
51. Tanaka, H.; Ono, G.; Nagano, T.; Ohkubo, N. Electric power generation using piezoelectric resonator for power-free sensor node. In Proceedings of the Proceedings of the IEEE 2005 Custom Integrated Circuits Conference, 2005. IEEE. https://doi.org/10.1109/cicc.2005.1568617.
52. Elvin, N.G.; Lajnef, N.; Elvin, A.A. Feasibility of structural monitoring with vibration powered sensors. *Smart Materials and Structures* **2006**, *15*, 977–986. https://doi.org/10.1088/0964-1726/15/4/011.
53. Fang, H.B.; Liu, J.Q.; Xu, Z.Y.; Dong, L.; Wang, L.; Chen, D.; Cai, B.C.; Liu, Y. Fabrication and performance of MEMS-based piezoelectric power generator for vibration energy harvesting. *Microelectronics Journal* **2006**, *37*, 1280–1284. https://doi.org/10.1016/j.mejo.2006.07.023.
54. Lefeuvre, E.; Badel, A.; Richard, C.; Petit, L.; Guyomar, D. Optimization of Piezoelectric Electrical Generators Powered by Random Vibrations **2007**. https://doi.org/10.48550/ARXIV.0711.3309.
55. Kok, S.L.; White, N.M.; Harris, N.R. A novel piezoelectric thick-film free-standing cantilever energy harvester. In Proceedings of the Eurosensors XXII (06/09/08 - 10/09/08), 2008. Event Dates: 07 - 11 September 2008.
56. Shen, D.; Park, J.H.; Ajitsaria, J.; Choe, S.Y.; Wikle, H.C.; Kim, D.J. The design, fabrication and evaluation of a MEMS PZT cantilever with an integrated Si proof mass for vibration energy harvesting. *Journal of Micromechanics and Microengineering* **2008**, *18*, 055017. https://doi.org/10.1088/0960-1317/18/5/055017.
57. Zhu, D.; Beeby, S.; Tudor, J.; Harris, N. A Self Powered Tag for Wireless Structure Health Monitoring in Aeronautical Applications. In Proceedings of the PowerMEMS 2009 (01/12/09 - 04/12/09), 2009, pp. 201–204. Event Dates: 1-4 December 2009.
58. Wang, Z.L.; Song, J. Piezoelectric Nanogenerators Based on Zinc Oxide Nanowire Arrays. *Science* **2006**, *312*, 242–246. https://doi.org/10.1126/science.1124005.
59. Wang, X.; Song, J.; Liu, J.; Wang, Z.L. Direct-Current Nanogenerator Driven by Ultrasonic Waves. *Science* **2007**, *316*, 102–105. https://doi.org/10.1126/science.1139366.
60. Qiu, Y.; Zhang, H.; Hu, L.; Yang, D.; Wang, L.; Wang, B.; Ji, J.; Liu, G.; Liu, X.; Lin, J.; et al. Flexible piezoelectric nanogenerators based on ZnO nanorods grown on common paper substrates. *Nanoscale* **2012**, *4*, 6568. https://doi.org/10.1039/c2nr31031g.
61. Briscoe, J.; Jalali, N.; Woolliams, P.; Stewart, M.; Weaver, P.M.; Cain, M.; Dunn, S. Measurement techniques for piezoelectric nanogenerators. *Energy & Environmental Science* **2013**, *6*, 3035. https://doi.org/10.1039/c3ee41889h.
62. Al-Ruqeishi, M.S.; Mohiuddin, T.; Al-Habsi, B.; Al-Ruqeishi, F.; Al-Fahdi, A.; Al-Khusaibi, A. Piezoelectric nanogenerator based on ZnO nanorods. *Arabian Journal of Chemistry* **2019**, *12*, 5173–5179. https://doi.org/10.1016/j.arabjc.2016.12.010.

63. Jeong, S.J.; Kim, M.S.; Song, J.S.; kyung Lee, H. Two-layered piezoelectric bender device for micro-power generator. *Sensors and Actuators A: Physical* **2008**, *148*, 158–167. https://doi.org/10.1016/j.sna.2008.07.007.
64. Marzencki, M.; Ammar, Y.; Basrour, S. Integrated power harvesting system including a MEMS generator and a power management circuit. *Sensors and Actuators A: Physical* **2008**, *145-146*, 363–370. https://doi.org/10.1016/j.sna.2007.10.073.
65. Ma, S.; Fang, G.; Li, C.; Sheng, S.; Fang, L.; Fu, Q.; Zhao, X.Z. Controllable Synthesis of Vertically Aligned ZnO Nanorod Arrays in Aqueous Solution. *Journal of Nanoscience and Nanotechnology* **2006**, *6*, 2062–2066. https://doi.org/doi:10.1166/jnn.2006.354.
66. Manekkathodi, A.; Lu, M.Y.; Wang, C.W.; Chen, L.J. Direct Growth of Aligned Zinc Oxide Nanorods on Paper Substrates for Low-Cost Flexible Electronics. *Advanced Materials* **2010**, *22*, 4059–4063, [https://onlinelibrary.wiley.com/doi/pdf/10.1002/adma.201001289]. https://doi.org/https://doi.org/10.1002/adma.201001289.
67. Garcia, A.J.L.; Jalabert, T.; Pusty, M.; Defoor, V.; Mescot, X.; Montanino, M.; Sico, G.; Loffredo, F.; Villani, F.; Nenna, G.; et al. Size and Semiconducting Effects on the Piezoelectric Performances of ZnO Nanowires Grown onto Gravure-Printed Seed Layers on Flexible Substrates. *Nanoenergy Advances* **2022**, *2*, 197–209. https://doi.org/10.3390/nanoenergyadv2020008.
68. Ko, W.; Lee, S.; Myoung, N.; Hong, J. Solution processed vertically stacked ZnO sheet-like nanorod p–n homojunctions and their application as UV photodetectors. *J. Mater. Chem. C* **2016**, *4*, 142–149. https://doi.org/10.1039/C5TC02977E.